1200-km Transmission of 4096-ary Eigenvalue-modulated Signal Using a Neural Network-based Demodulator and SD-FEC

Ryotaro Harada[1], Tsuyoshi Yoshida[2], Daisuke Hisano[1], Akihiro Maruta[1], and Ken Mishina[1,*]

[1] *Graduate School of Engineering, Osaka University, 2-1 Yamada-oka, Suita, Osaka 565-0871, Japan*
[2] *Information Technology R&D Center, Mitsubishi Electric Corporation, Kamakura 247-8501, Japan*
[*] *e-mail: mishina@comm.eng.osaka-u.ac.jp*

Abstract: We experimentally demonstrate the transmission of a 4096-ary eigenvalue-modulated signal using a neural network-based demodulator and SD-FEC. The experimental results indicate a successful operation with an error-free transmission through a 1200-km optical fiber line.

1. Introduction

Optical eigenvalue modulation [1] using the inverse scattering transform (IST) [2] has gained considerable attention as a theoretical framework to overwhelm the nonlinear Kerr limit in optical fiber communication systems [3]. The IST is well-known as nonlinear Fourier transform (NFT). To increase the transmission capacity, various IST-based transmission methods using multilevel and multieigenvalue modulations have been demonstrated, e.g., 64-QAM of the nonlinear spectrum [4] and on–off encoding [5] of multieigenvalue. We proposed a 4096($= 2^{12}$)-ary eigenvalue-modulated signal using an on–off encoding of 12 eigenvalues as high-order multilevel modulation; however, the transmission distance demonstrated in the experiment was only 50 km [6].

The transmission distance of IST-based communication systems is generally limited by noise and dispersion effects including inter-symbol interference [7]. To improve the noise tolerance, several machine learning-based approaches have been studied [8]. For the on–off encoding, an eigenvalue-domain (ED) neural network (NN)-based receiver has been demonstrated [9]. In addition, the application of soft-decision forward error correction (SD-FEC) techniques to a 16-ary eigenvalue modulated signal, which used a multilabel NN to compute the L-value, has been proposed to extend the transmission distance [10]. However, the applicability of the multilabel NN receiver with SD-FEC to high multilevel modulation, such as 4096-ary modulation, is yet to be studied.

In this study, we numerically and experimentally investigate the applicability of the multilabel ED-NN receiver and SD-FEC to a 4096-ary eigenvalue-modulated signal to extend the transmission distance. We demonstrate that SD-FEC with the multilabel NN receiver can be applied using an appropriate NN training condition even for the 4096-ary signal. Moreover, we employ a non-zero dispersion-shifted fiber (NZ-DSF) with a small dispersion parameter of 0.7 ps/nm/km to suppress distortions due to the dispersion effect. Finally, we successfully achieve the extension of the transmission distance to 1200 km even for the 4096-ary eigenvalue-modulated signal.

2. Eigenvalue Modulation and SD-FEC Using NN-based Demodulator

In this study, we employed a multieigenvalue transmission system using an on–off encoding of 12 eigenvalues [6]. Fig. 1(a) illustrates an overview of this multieigenvalue transmission system. At the transmitter, a 12-bit sequence is encoded into an eigenvalue pattern. On–off encoding is based on a one-to-one mapping between a 12-bit input and a subset of eigenvalues. For a bit value of 1 (or 0) at the j-th position b_j, the j-th eigenvalue $\zeta^{(j)}$ is included (or excluded). The eigenvalue pattern is then converted into a pulse using the IST. When the number of eigenvalues is N, the converted pulse corresponds to the N-soliton solution. The numbers of eigenvalue and pulse patterns are $2^{12} = 4096$. The 4096-ary eigenvalue-modulated signal is then transmitted through the fiber. Although the pulse shape and spectrum change by dispersion and Kerr nonlinearity during the fiber transmission, the eigenvalue pattern is invariant.

At the receiver, a complex envelope amplitude of the received pulse is obtained by a coherent receiver. An eigenvalue pattern is detected from the pulse by using the IST. The detected eigenvalue pattern is decoded into a bit sequence of 12 bits. Note that eigenvalue detection is processed symbol by symbol. Therefore, the detected eigenvalue pattern is distorted when the guard time between symbols is insufficient and an inter-symbol interference occurs due to the dispersion effect.

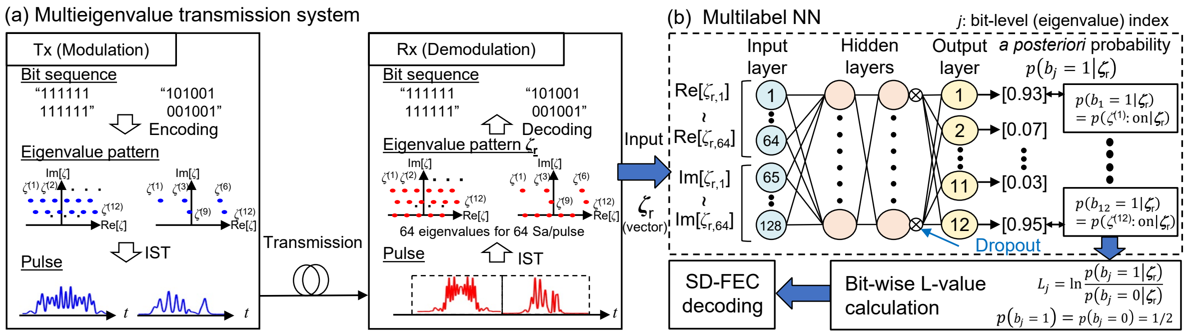

Fig. 1: Overview of (a) multieigenvalue transmission system and (b) multilabel NN demodulator for SD-FEC.

For demodulation and decoding, we applied SD-FEC to the 4096-ary eigenvalue-modulated signal using the concept in [10]. In the eigenvalue modulation, the derivation of the L-value is difficult because the eigenvalues obtained via the IST do not exactly follow a Gaussian distribution [11]. In this study, we employed a multilabel NN to compute the L-value for SD-FEC. Fig. 1(b) presents an overview of the demodulation and SD-FEC decoding for the 4096-ary eigenvalue-modulated signal. The detected eigenvalue vector $\boldsymbol{\zeta}_{\mathrm{r}}$, consisting of the real and imaginary parts of the eigenvalues, was input to the multilabel NN. The number of output units was set to 12 which corresponds to the number of eigenvalues (number of bits) for the on–off encoding. A logistic sigmoid function and a cross-entropy error function were used as the output and loss function, respectively. *A posteriori* probability of the on-state of the j-th eigenvalue $\zeta^{(j)}$, namely $p(b_j = 1|\boldsymbol{\zeta}_{\mathrm{r}})$, was obtained at each unit. The bit-wise L-value L_j could be calculated from the ratio of $p(b_j = 1|\boldsymbol{\zeta}_{\mathrm{r}})/p(b_j = 0|\boldsymbol{\zeta}_{\mathrm{r}})$, which was input to the SD-FEC decoder.

3. Simulations

We performed a numerical simulation for a back-to-back configuration to investigate the applicability of the combination of the multilabel NN and SD-FEC to a 4096-ary eigenvalue-modulated signal. Fig. 2(a) depicts the simulation model. The on-off encoding of the triangular-lattice-shaped 12 eigenvalues was employed as in our previous work [6]. For the eigenvalue-modulated signal, we prepared a pulse sequence by shuffling the 4096 pulses randomly. The pulse duration was set to 1.07 ns, and the bit rate with an overhead of the SD-FEC was 11.25 Gb/s. At the receiver, the signal was demodulated using the multilabel NN receiver at 60 GSa/s, which corresponded to 64 samples per pulse. Two hidden layers with 512 hidden units and a rectified linear unit (ReLU) activation function were employed in the NN. The bit-wise L-value was computed using the multilabel NN-based demodulator as described in the previous section. The numbers of the training and test samples were 16384 and 65536, respectively. The NN was trained using the Adam optimizer [12] by employing the early stopping algorithm. Two training conditions were examined: The NN was trained (i) for each optical signal-to-noise ratio (OSNR) using each OSNR data and (ii) using the OSNR data in the vicinity of the SD-FEC limit (OSNR=1.3 dB). For SD-FEC, we used the DVB-S2 low-density parity check code (LDPC) [13] with the overhead (OH) of 20%. The number of decoding iterations for SD-FEC was optimized within the range of 1 to 10.

Fig. 2(b) shows the bit error rate (BER) characteristics before and after SD-FEC. The BER characteristics were improved by using SD-FEC under both conditions. The BER before SD-FEC for condition (i) was better than that for condition (ii). However, residual errors were observed for condition (i) because the NN was trained inadequately. For condition (i), the NN demodulator using the data of high OSNR, wherein the data far from the ideal signal points are not included, could not process noisy data and outliers. In contrast, a clear waterfall curve without residual errors was obtained for condition (ii). These trends correspond to the results for the 16-ary eigenvalue-modulated signal in [10]. Thus, the multilabel NN and SD-FEC can be applied to the 4096-ary eigenvalue-modulated signal by using the appropriate training conditions.

In addition, to investigate the feasibility of the long-haul transmission of the 4096-ary eigenvalue-modulated signal, we performed a transmission simulation based on the split-step Fourier method. Two NZ-DSFs of $D = 4.4$ and 0.7 ps/nm/km were examined to suppress the dispersion effects for long-haul transmission. The NZ-DSF parameters were a dispersion slope of S =0.063 ps/nm^2/km, a nonlinear coefficient of $\gamma = 2.4$ W^{-1}/km, and a fiber loss of 0.21 dB/km. The transmission line consisted of a 40-km NZ-DSF and an erbium-doped fiber amplifier (EDFA). Fig. 2(c) shows the BER characteristics before SD-FEC after the transmission. For $D = 4.4$ ps/nm/km, the BER was significantly degraded after the 400-km transmission. The detected eigenvalue pattern, which included all 4096 patterns, was distorted due to the inter-symbol interference, as shown in Fig. 2(c). For $D = 0.7$ ps/nm/km, the BER below the SD-FEC limit (AWGN, OH 20%) with a small OSNR penalty could be achieved even after the 400-km transmission. The NZ-DSF with a small dispersion parameter of $D = 0.7$ ps/nm/km is suitable for the long-haul transmission of the 4096-ary eigenvalue-modulated signal.

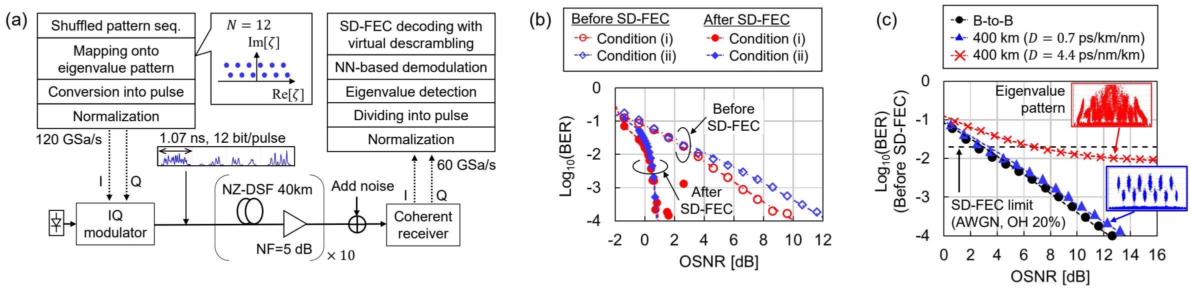

Fig. 2: (a) Simulation model. (b) BER before and after SD-FEC for B-to-B. (c) BER characteristics before SD-FEC after the transmission.

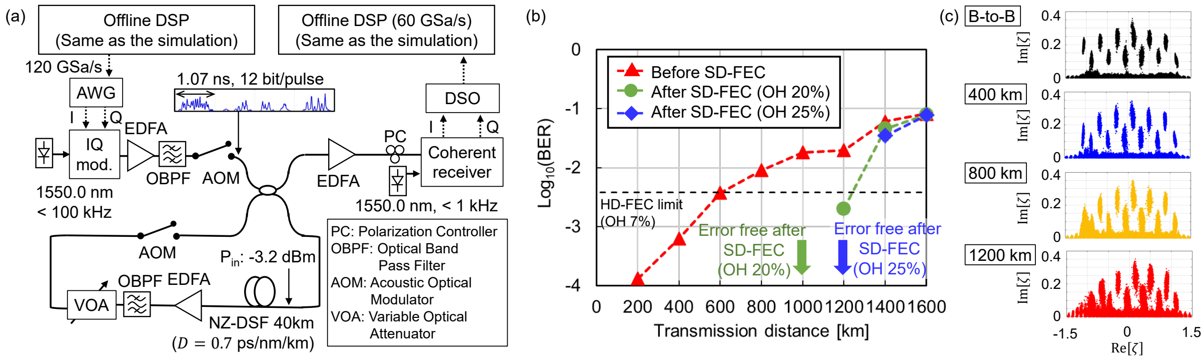

Fig. 3: (a) Experimental setup. (b) BER before and after SD-FEC and (c) eigenvalue patterns with varying transmission distances.

4. Experiments

Fig. 3(a) depicts the experimental setup with an offline digital signal processing (DSP) including the multilabel NN demodulator and SD-FEC decoder. For eigenvalue modulation/demodulation and decoding, the same parameters that were used in the simulations were considered. The eigenvalue-modulated optical signal was generated using an arbitrary waveform generator (AWG) and IQ modulator. The optical signal was launched into a transmission loop, which consists of 40-km NZ-DSF of $D = 0.7$ ps/nm/km and an EDFA. The other parameters of the NZ-DSF were identical to those in the simulation. At the receiver end, the digital IQ signals were obtained by using a coherent receiver and a digital storage oscilloscope (DSO). The DSP for demodulation was performed offline at 60 GSa/s. The NN was trained using condition (ii).

Fig. 3(b) shows the BER before and after SD-FEC with varying transmission distances in the experiment. Fig. 3(c) shows the detected eigenvalue patterns that include all 4096 patterns after the transmission. The BER and the eigenvalue pattern gradually degraded due to the dispersion and noise effects as the transmission distance increased. In particular, the eigenvalues around edges ($\mathrm{Re}[\zeta] = \pm 1.1$) were distorted because these eigenvalues corresponded to the edges of the pulse in the time domain and high-frequency components. Assuming that HD-FEC with an OH of 7% was used for decoding, the achievable transmission distance was approximately 600 km. On the other hand, owing to the multilabel NN and SD-FEC, an error-free operation was achieved even after a 1000-km transmission. By using SD-FEC with an OH of 25%, an achievable transmission distance could be extended to 1200 km. We expect that a longer transmission distance than 1200 km will be achieved by suppressing the eigenvalue distortion around the edges, e.g., using a highly dense eigenvalue pattern in the real axis direction.

5. Conclusions

We experimentally demonstrated the transmission of a 4096-ary eigenvalue-modulated signal using the on–off encoding of 12 eigenvalues. Successful error-free transmission over 1200 km at 11.25 Gb/s was achieved using a multilabel NN demodulator, SD-FEC, and an NZ-DSF with a low dispersion parameter of $D = 0.7$ ps/nm/km.

Acknowledgments This work was supported by the commissioned research of NICT, Japan, grant number 01401.

References

1. A. Hasegawa et al., J. Lightw. Technol., **11**, 395–399 (1993).
2. M. J. Ablowitz and H. Segur, *Solitons and the Inverse Scattering Transform* (SIAM, 1981).
3. S. K. Turitsyn et al., Optica, **4**, 307–322 (2017).
4. S. T. Le et al., Nature Photonics., **11**, 570–577 (2017).
5. S. Hari et al., J. Lightw. Technol., **34**, 3110–3117 (2016).
6. K. Mishina et al., in Proc. OFC2021, Paper M3I.1 (2021).
7. S. Civelli et al., Photon. Technol. Lett., **29**, 1332–1335 (2017).
8. P. Freire et al., Adv. Opt. Photon., **15**, 739–834 (2023).
9. K. Mishina et al., J. Lightw. Technol., **39**, 4307–4317 (2021).
10. K. Mishina et al., in Proc. ECOC2023, Paper Th.B.5.4 (2023).
11. S. Wahls et al., in Proc. SCC2017, 1–6 (2017).
12. D. Kingma and J. Ba, in Proc. ICLR2015, pp. 1–15 (2015).
13. ETSI., EN 302 307-1, v.1.4.1 (2014).